

EV Fleet Flexibility Estimation and Forecasting for V2X Applications

Chaimaa Essayeh, Amin Vilan, Omid Homaei, and Vahid Vahidinasab, *Senior Member, IEEE*

Abstract—Forecasting the flexibility potential of Vehicle-to-Everything (V2X) systems is important for the future of energy networks, where the integration of renewable energy sources and electric vehicles poses significant challenges. In this paper, we present a novel method for estimating and predicting V2X flexibility potential of an EV fleet, based on an aggregate polytope representation, addressing the need for accurate and reliable forecasting methods in the realm of sustainable transportation. The method is robust against individual uncertainties of EV owners behaviours as it is applied at an aggregate level, and the reformulation of the V2X potential as a set of linear constraints allows the proposed method to be integrated into different optimisation problems and therefore be applied for diverse V2X applications. Case studies showcase the capability of the method in capturing the V2X flexibility potential and demonstrate its effectiveness for different V2X applications.

Index Terms—V2X, Smart Grid, Local Flexibility Market, DSO

I. INTRODUCTION

The transportation sector, one of the largest contributors to greenhouse gas emissions [1] due to its major reliance on fossil fuels, is undergoing a significant transition driven by government policies aimed at reducing climate change and pollution [2]. Electrification of transportation, particularly through Battery Electric Vehicles (BEVs) powered by renewable energy, is seen as a key solution for cutting emissions and improving air quality in cities [3]. While the shift is still in its early stages, advancements in battery technology have resulted in larger capacities and lower costs, making EVs more accessible. This trend is expected to accelerate, with countries like the UK projected to have up to 28 million EVs on the road by 2035 [4].

This level of electrification will significantly impact the operation of electrical energy systems. The primary challenge will be the substantial increase in electrical energy demand required to supply EVs. For instance, the transportation sector accounts for roughly 36% of energy consumption in the UK. Transitioning this energy demand to electrical networks would create considerable challenges related to generation, transmission, and distribution [5]. From a more technical point of view, this could lead to voltage stability and power quality issues, which have been thoroughly reviewed in [6, 7], and may necessitate the deployment of costly grid reinforcement.

Although this transition in the transportation sector presents significant challenges for the energy sector, it also offers several opportunities. EV batteries can serve as mobile energy storage systems that can be used to facilitate the integration of intermittent renewable energy resources [8, 9], support the system in high demand load periods [10] and supply backup power during outages. Unlocking the EV flexibility potential offers a cost-effective solution to grid reinforcement, generates new revenue streams for end-customers and enhances EVs' role in modernizing and stabilizing the energy system. To effectively harness the benefit of this flexibility, it is essential to develop various flexibility mechanisms. Particularly, and due to the uncertain behaviour of EVs' owners, accurate EV flexibility estimation and forecasting methods will play a pivotal role in the adoption of such flexibility.

To provide a reliable foundation for flexibility forecasting, robust estimation methods are essential. In [11], flexibility is estimated by multiplying the charging station's utilization rate, the power capacity of the charging ports, and the service duration. This method assumes that the operator can draw power equivalent to the charging port's capacity from each connected EV. However, if an EV has just been plugged in with a minimal state of charge (SOC_{min}), extracting V2X power could push it below the recommended minimum level. Likewise, if the EV has already reached its maximum state of charge (SOC_{max}), the approximate formula implies that the EV can be charged beyond this limit, simply because it is plugged in and theoretically capable of being charged or discharged at the port's power rate. An enhanced estimation method was used in [12], that instead of using the service duration to estimate the flexibility used the idle period. The study estimated flexibility by computing the required charging time to reach the desired energy level and subtracting it from the EV's availability period, assuming the remaining idle period can be used for flexibility. However, this assumption overlooks user preferences and technical constraints. For example, if an EV reaches full charge at time t and is scheduled to depart at $t + 1$, the method incorrectly considers this final time slot as available for flexibility. Charging is not possible because the battery is already full, and discharging would leave the EV with less than the desired charge level, conflicting with the user's needs. Thus, this approach risks overestimating the actual flexibility potential. In their approach, [13] presented a more accurate model for flexibility estimation. The flexibility potential of a carpark is estimated by first calculating the baseline schedule for each EV and then using linear programming to compute the available flexibility over a specific time window, followed by summing the individual

C. Essayeh and O. Homaei are with the Department of Engineering, Nottingham Trent University, United Kingdom.

A. Vilan is with the Islamic Azad University, Tehran, Iran

V. Vahidinasab is with the Business School, University of Salford

Corresponding author e-mail: v.vahidinasab@salford.ac.uk

Manuscript received Month xx, yyyy; revised Month xx, yyyy.

flexibilities to estimate the aggregate flexibility. However, this method presents several limitations. Assuming the same baseline for all EVs is unrealistic, as individual behaviors vary significantly. Moreover, computing flexibility for each EV in every time window requires re-running the procedure for all windows, which becomes computationally expensive. The studies in [14, 15] modeled the power and energy boundaries of an entire fleet using min/max expressions. While simple and accurate, this method is limited in capturing complex inter-dependencies and multi-dimensional constraints. Moreover, it doesn't scale as effectively for large systems or detailed optimization tasks. In [16], a stochastic optimization approach is used to develop an aggregation model that captures the flexibility potential of EV parking lots. The model estimates the parking lot's maximum flexibility margins (downstream and upstream) in advance, however, it does not capture the power boundaries and the minimum level capacities for the EVs. A polytope-based aggregation approach was introduced in [17], offering accurate modeling of time-coupled and heterogeneous individual EV behaviors. However, the method is limited to aggregating EVs with identical arrival and departure times, making it unsuitable for capturing the diversity of charging demands or estimating flexibility across different times of the day. Additionally, it requires multiple iterations of the aggregation process, leading to higher computational costs for the aggregator.

Building on these estimation techniques, accurate forecasting of flexibility is crucial for real-time applications and operational planning. In [18], forecasting models including ridge regression, K-nearest neighbors (kNN), Gaussian processes (GP), Support Vector Regression (SVR), and Artificial Neural Networks (ANN), were employed to improve the flexibility forecasting. However, due to the limitations of these models that can only learn a single target variable at a time, an iterative prediction approach was applied to generate forecasts over multiple time steps. Similarly, [19] employed techniques such as naive benchmarks, quantile regression, and kernel density estimation to forecast EV flexibility. In [20], the accuracy and performance of Gaussian mixture models and LightGBM were assessed. However, these approaches remain limited as they typically rely on a single-output or cluster-based frameworks that do not address multivariate, multi-step interdependent forecasting as effectively as deep learning approaches.

In [21], SVR models were used for predicting aggregated EV flexibility. The two-step forecasting model predicts the aggregate charging profile within the flexibility request window, and the second step predicts the available flexibility in the same time window. Similarly, in [22], a combination of transformers and temporal convolution networks (TCNs) was used to forecast aggregated flexibility of an EV aggregator. Although the forecasting models in both papers were advanced and accurate, the underlying flexibility estimation strategy was restricted by its reliance on specific baselines and predefined flexibility services. Each unique combination of baseline and flexibility type (upstream or downstream) requires separate calculations and retraining, making it resource-intensive and less adaptable for varied scenarios. Moreover, the flexibility forecast becomes rigidly tied to predefined conditions, limiting

its general applicability and scalability for dynamic energy market needs.

This paper presents novel methods for estimating and forecasting V2X flexibility potential of an EV fleet, based on an aggregate polytope representation. The methods are robust against individual uncertainties of EV owners behaviours as they are applied at an aggregate level, and the reformulation of the V2X potential as a set of linear constraints allows the proposed methods to be integrated into different optimisation problems and therefore be applied for diverse V2X applications. We summarise the novelty of the paper as follow:

- We propose a novel method for estimating V2X flexibility potential of an EV fleet based on a polytope representation,
- We leverage advanced multi-variate input multi-step multi-variate output deep learning techniques for an accurate forecasting of V2X flexibility of an EV fleet,
- We present examples of application of both V2X estimation and V2X forecasting to showcase the capabilities of both methods.

The paper is structured as follows: In Section II, a mathematical model is introduced to estimate V2X potential at an aggregate level. In Section III, state-of-the-art forecasting algorithms are leveraged to accurately predict V2X potential for future time horizons. The effectiveness of the method across diverse V2X applications is showcased in Section IV through a couple of case studies. Finally, Section V concludes the paper and discusses potential directions.

II. V2X FLEXIBILITY ESTIMATION

The operational constraints of a battery can be expressed in a polytope form [23]: $\{p|Ap \leq b\}$, with p is the power schedule of the battery and A and b are as follows:

$$A = \begin{bmatrix} \mathbf{I} & \mathbf{0} \\ -\mathbf{I} & \mathbf{0} \\ \mathbf{0} & \mathbf{I} \\ \mathbf{0} & -\mathbf{I} \\ (\eta_{in}\delta t)\Gamma & (\eta_{out}\delta t)\Gamma \\ -(\eta_{in}\delta t)\Gamma & -(\eta_{out}\delta t)\Gamma \end{bmatrix}$$

$$\Gamma = \begin{bmatrix} 1 & 0 & 0 & \dots & 0 \\ \alpha & 1 & 0 & \dots & 0 \\ \alpha^2 & \alpha & 1 & \dots & 0 \\ \vdots & \vdots & \vdots & \ddots & \vdots \\ \alpha^{T-1} & \alpha^{T-2} & \alpha^{T-3} & \dots & 1 \end{bmatrix}$$

$$b = \begin{bmatrix} P_{max} \\ \mathbf{0} \\ \mathbf{0} \\ -P_{min} \\ C_{max} - \alpha C_0 \\ \vdots \\ C_{max} - \alpha^T C_0 \\ \alpha C_0 - C_{min} \\ \vdots \\ \alpha^T C_0 - C_{min} \end{bmatrix}$$

TABLE I: Description of the parameters in matrix A and vector b

Parameter	Description
α	self-discharging rate
η_{in}, η_{out}	charging, discharging efficiency
$\mathbf{P}_{max}, \mathbf{P}_{min}$	maximum, minimum charging rate vectors
C_{max}, C_{min}	Maximum and minimum allowed energy levels
C_0	Initial energy level of the battery at time step $t = 0$
C_{arr}, C_{dep}	Energy levels of the EV battery at arrival and departure

The parameters figuring in the matrix A and vector b are the technical parameters of the battery and are summarized in Table I. \mathbf{I} and $\mathbf{0}$ are respectively the unity and zero vectors of size T , with T being the time horizon for the battery operation, and δt the time step of the operation. The first two blocks of the constraint $Ap \leq b$ define the upper and lower bounds on the charging rate of the battery. Similarly, the second two blocks define the upper and lower limits on the discharging rates, and the final two blocks limits the battery capacity in the range of its maximum and minimum capacity allowance. Hence, the size of A is $(6T, 2T)$ and b is $(6T, 1)$.

With relevant adjustments, the battery model can be adopted for EVs:

- 1) The vector elements of \mathbf{P}_{max} and \mathbf{P}_{min} in the time slots where the EV is not available will be equal to zero.
- 2) C_0 for a battery is equivalent to the capacity at arrival C_{arr} for an EV.
- 3) the last $T - t_{dep}$ rows of vector b can be modified to $\alpha^{t_{dep}+i}C_{arr} - C_{dep}$ to force the battery to be charged at least at the desired level C_{dep} at time of departure t_{dep} .
- 4) The first $[0-t_{arr}]$ elements of the minimum capacity limit block are set to 0.

With these cited adjustments, vector b becomes:

$$b_{ev} = \begin{bmatrix} \mathbf{P}_{max} \\ \mathbf{0} \\ \mathbf{0} \\ -\mathbf{P}_{min} \\ \hline 0 \\ \vdots \\ 0 \\ C_{max} - \alpha C_{arr} \\ \vdots \\ C_{max} - \alpha^{t_{dep}-t_{arr}} C_{arr} \\ \vdots \\ C_{max} - \alpha^{t_{dep}-t_{arr}} C_{arr} \\ \hline 0 \\ \vdots \\ 0 \\ \alpha C_{arr} - C_{min} \\ \vdots \\ \alpha^{t_{dep}-t_{arr}} C_{arr} - C_{dep} \\ \vdots \\ \alpha^{t_{dep}-t_{arr}} C_{arr} - C_{dep} \end{bmatrix}$$

To enhance readability, horizontal lines were added to separate

the power bounds block from the maximum capacity limit block and the minimum capacity limit block. Following the demonstration in [23], an aggregation of EVs $(EV_i)_{i \in [1, N]}$ can also be represented as a polytope:

$$\{p_{agg} | A_{agg} p_{agg} \leq b_{agg}\}$$

Assuming all EVs in the aggregation have the same self discharge rate α and the same charging/discharging efficiencies η_{in}/η_{out} , matrix A will be the same for all EVs, and the aggregate polytope can be expressed as:

$$P = \{p_{agg} | A_{agg} p_{agg} \leq b_{agg}\} \quad (1)$$

with:

$$\begin{cases} A_{agg} = A = A_1 = A_2 = \dots = A_N \\ p_{agg} = \sum_{i=1}^N \mathbf{p}_i \\ b_{agg} = \sum_{i=1}^N b_i \end{cases}$$

In a compact form b_{agg} can be written as:

$$b_{agg} = \begin{bmatrix} \mathbf{P}_{max}^{agg} \\ \mathbf{0} \\ \mathbf{0} \\ -\mathbf{P}_{min}^{agg} \\ \mathbf{C}_{max}^{agg} \\ \mathbf{C}_{min}^{agg} \end{bmatrix} = \begin{bmatrix} \sum_{i=1}^N \mathbf{P}_{max}^i \\ \mathbf{0} \\ \mathbf{0} \\ -\sum_{i=1}^N \mathbf{P}_{min}^i \\ \sum_{i=1}^N \mathbf{C}_{max}^{i'} \\ \sum_{i=1}^N \mathbf{C}_{min}^{i'} \end{bmatrix}$$

with:

$$\mathbf{C}_{max}^{i'} = \begin{bmatrix} 0 \\ \vdots \\ 0 \\ C_{max}^i - \alpha C_{arr}^i \\ \vdots \\ C_{max}^i - \alpha^{t_{dep}-t_{arr}} C_{arr}^i \\ \vdots \\ C_{max}^i - \alpha^{t_{dep}-t_{arr}} C_{arr}^i \end{bmatrix}$$

and

$$\mathbf{C}_{min}^{i'} = \begin{bmatrix} 0 \\ \vdots \\ 0 \\ \alpha C_{arr}^i - C_{min}^i \\ \vdots \\ \alpha^{t_{dep}-t_{arr}} C_{arr}^i - C_{dep}^i \\ \vdots \\ \alpha^{t_{dep}-t_{arr}} C_{arr}^i - C_{dep}^i \end{bmatrix}$$

We note that the assumption of similar self discharge rate and charging/discharging efficiencies is a reasonable approximation for the following reasons:

- Aggregation smooths individual variabilities: variations in individual EV parameters tend to cancel each other out, making the collective behavior more stable and

less sensitive to minor differences between individual vehicles,

- Standardization of EV battery models: Advances in battery technology have led to convergence in the efficiency of charging and discharging processes across different EVs, reducing the magnitude of variability. Many EVs are composed of standardized battery models with comparable parameters, making the considered assumptions realistic and consistent with industry trends.

At the bulk system or transmission system level, this method offers several significant benefits. By capturing the collective behavior of a large fleet of EVs, the aggregation approach enables the system operator to treat the entire fleet as a single, flexible resource that can be utilized to support grid stability and efficiency. The aggregated model allows for the incorporation of the fleet's flexibility into system-wide optimization problems, such as those related to balancing supply and demand, managing congestion, or integrating renewable energy sources. This enhances the ability to respond to market signals or grid emergencies with greater precision, offering a scalable solution that can be integrated into broader grid management strategies. Similarly, if we consider a charging station with N EVs, the set of linear constraints $A_{agg}p_{agg} \leq b_{agg}$ captures all the technical requirements of the EV fleet over the considered time horizon T , and can therefore be included in any optimisation problem to schedule the charging/discharging operations of the charging station in response to a market signal or an incentive while respecting the operational constraints of the EV batteries. In other words, solving an optimisation problem with system (1) provides the charging station operator with insights into the potential discharging capacity that can be deployed to the grid at each time step t , while ensuring compliance with EVs constraints, and potentially other constraints embedded within the optimization problem (e.g., network constraints). We note that solving a problem that incorporates the aggregate polytope constraints will return an aggregate solution p_{agg} at an aggregate level. The formula that recovers a feasible solution \mathbf{p} from an approximate aggregate solution p_{agg} is presented in [23] and is as follows:

$$\begin{aligned} \min_{p_i, i=1, \dots, N} \quad & \left\| p_{agg} - \sum_{i=1}^N p_i \right\| \\ \text{s.t.} \quad & A_i p_i \leq b_i, \quad i = 1, \dots, N \end{aligned} \quad (2)$$

A. Example

We work with the *Crowd Charge* dataset [24], a dataset that collected charging session data from approximately 700 EV owners who participated in an 18-month trial for a home smart charging initiative conducted in the UK. This dataset was selected because it is the only open-source dataset that has recorded the capacity of the tracked EV batteries C_{max} , essential for the construction of the individual b_{ev} vectors. The capacity at arrival C_{arr} and the desired capacity at departure C_{dep} are not available in the dataset and were approximated as shown in Eqs. (3), with C_{cons} (kWh) is the consumed energy during the session. We select a horizon of one day with 15 min

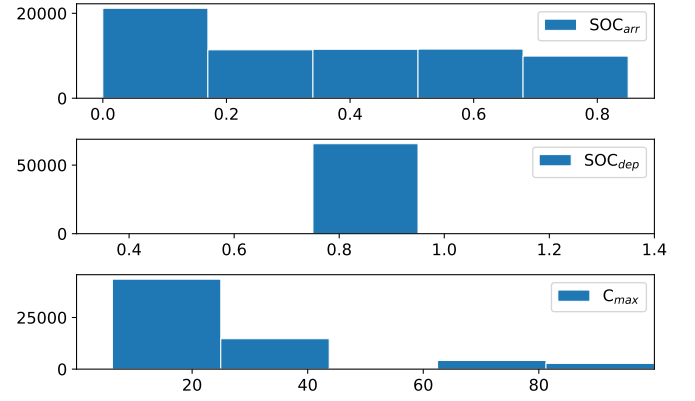


Fig. 1: Overview of the EVs statistics for the considered dataset: The majority of the cars come with a SOC_{arr} less than 0.2 and leave with a SOC greater than 0.8. The battery capacities are concentrated around 20 kWh with few of them in the range of 40, 80 and 100 kWh.

resolution. Since b_{ev} is formulated over a finite horizon T (i.e., one day in our case) and the EV availability can span across multiple days, particularly in the case of home charging, we supposed that the battery capacity at the end of a day should be proportional to the final desired capacity. For example, if an EV arrives with a capacity C_{arr} , wants to leave with a capacity C_{des} , and is parking for 6 time slots, with 4 time slots on day 1 and 2 time slots in day 2, then $C_{arr}^{day1} = C_{arr}$, $C_{des}^{day1} = \frac{4}{6}C_{des}$, $C_{arr}^{day2} = C_{des}^{day1}$ and $C_{des}^{day2} = C_{des}$. Figure 1 gives an overview of the different EV batteries information following the application of the mentioned approximations. Most EVs arrive with a state of charge SOC_{arr} around 0-0.2%, and depart with a SOC_{dep} of 0.8% or larger. The EVs that participated in the trial have capacities ranging between 20 kWh to 100 kWh, with the majority concentrated around the 20 kWh. The b_{ev} vectors are then constructed using OPLEM platform [25] and summed up according to Eq. 1 to return b_{agg} . The source code for computing b_{agg} can be found in the Github repository of the project¹. Figure 2 displays the aggregate maximum charging/discharging rates and the aggregate maximum/minimum capacities for the duration of the project trial between 01 March 2017 and 01 January 2019. Roughly speaking, an aggregator managing this fleet of EVs can be seen as an EV with 500 kW maximum charging rate, 4000 maximum capacity and around 2000 minimum capacity. An example demonstrating how can we leverage such information to gain insights is presented in the first case study of Section IV.

III. V2X FLEXIBILITY FORECASTING

In real-world applications, transmission system operators and EV aggregators such as charging station operators (CSOs) must assess the availability and demand of EVs ahead of time to effectively allocate resources. As the vector b_{agg} captures all the technical constraints of an aggregate EV fleet, we assess in this paper the capability of forecasting b_{agg} using advanced forecasting models.

¹<https://github.com/GridLab-NTU/V2X-prediction>

$$\begin{cases} C_{arr} = 0.2C_{max} & \text{and} & C_{dep} = C_{arr} + C_{cons} & \text{if} & 0.2C_{max} + C_{cons} \leq C_{max} \\ C_{arr} = C_{max} - C_{cons} & \text{and} & C_{dep} = C_{max} & \text{if} & 0.2C_{max} + C_{cons} > C_{max} \\ C_{min} = 0 \end{cases} \quad (3)$$

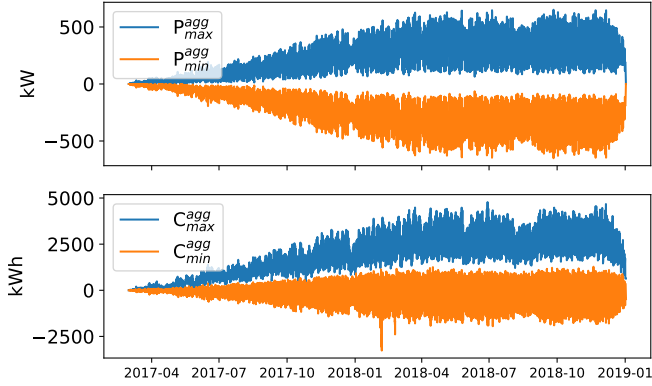


Fig. 2: The vectors of the constructed b_{agg} from the considered dataset. P_{min}^{agg} is equivalent to the negative value of P_{max}^{agg} as we considered that the EVs have symmetrical charging/discharging capacities. Roughly, the aggregator can be seen as an EV with 500 kW maximum charging rate and 4000 maximum capacity.

A. Setting

We use the same dataset as in the previous section and train different deep learning forecasting models to predict the day-ahead values of \mathbf{P}_{max}^{agg} , \mathbf{C}_{max}^{agg} and \mathbf{C}_{min}^{agg} vectors. \mathbf{P}_{min}^{agg} was not forecasted as it is equal to the negative value of \mathbf{P}_{max}^{agg} . For EV fleet containing EVs with asymmetric charging/discharging rates, \mathbf{P}_{min}^{agg} should be also predicted. The training was conducted in two phases. In the first phase, we explored various deep learning (DL) architectures, including RNN, LSTM, bi-LSTM, and GRU, to identify the configurations that consistently delivered the best performance across different settings. The details of the explored architectures can be found in the Appendix A, Table V. Based on the results from this initial round, we selected attention-based CNN-LSTM and Transformer models for further evaluation. In the second phase, we performed hyperparameter tuning on these selected models to enhance their accuracy and optimize their predictive capabilities. The specifics of the models and the hyperparameters adjusted during tuning are detailed in the Appendix A, Table VI.

Our objective is to design a model capable of simultaneously forecasting three variables over a defined horizon T . Fig. 3 illustrates the general structure of this model. This model input consists of several vector variables (e.g., \mathbf{P}_{max}^{agg} , \mathbf{C}_{max}^{agg} and \mathbf{C}_{min}^{agg} in our case), each with n historical values. The model then forecasts multiple vectors as the output, where each output vector predicts a sequence of T future time steps over a lead time of k steps into the future. Unlike univariate output models, which require a separate model for each variable, this approach consolidates the forecasting process into a single model for all three variables, leveraging the relationships across both the different variables and the multiple time steps.

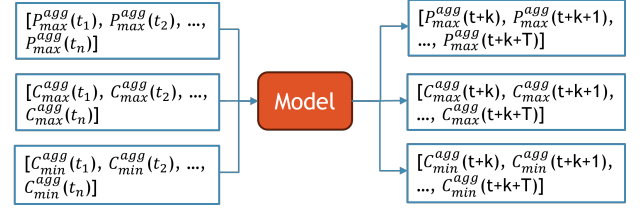


Fig. 3: Multivariate input multi-step multivariate output with n historical data, k lead time and T steps.

However, this integrated approach presents a greater challenge in training to achieve satisfactory accuracy.

The input data included values of the three main features: \mathbf{P}_{max}^{agg} , \mathbf{C}_{max}^{agg} and \mathbf{C}_{min}^{agg} , and is structured as follows:

- **Current Value:** The current values of the 3 variables \mathbf{P}_{max}^{agg} , \mathbf{C}_{max}^{agg} and \mathbf{C}_{min}^{agg} , namely, $P_{max}^{agg}(w, d, t)$, $C_{max}^{agg}(w, d, t)$ and $C_{min}^{agg}(w, d, t)$, with w referring to the index of the current week, d the current day and t to the current time slot.
- **Quarter-hourly History:** Values of the variables for the past 23 hours, capturing short-term dependencies. For \mathbf{P}_{max}^{agg} for instance, we have $P_{max}^{agg}(w, d, t - \delta t)$, ..., $P_{max}^{agg}(w, d, t - T)$.
- **Daily History:** Values of the variables for the same time across the past 6 days, capturing daily seasonality, e.g., $P_{max}^{agg}(w, d - 1, t + k)$, ..., $P_{max}^{agg}(w, d - 6, t + k)$.
- **Weekly History:** Values of the variables for the same time across the past 5 weeks, capturing weekly patterns, e.g., $P_{max}^{agg}(w - 1, d, t + k)$, ..., $P_{max}^{agg}(w - 5, d, t + k)$.
- **Target:** The models predict the 96 values of the three variables beginning from the k^{th} time slot ahead of the current moment, e.g., $P_{max}^{agg}(w, d, t + k)$, ..., $P_{max}^{agg}(w, d, t + k + 96)$.

We utilized Python, TensorFlow (DL models), and Scikit-learn (for baseline model) for model development and training. The models were trained using Google Colab, a cloud-based platform with NVIDIA Tesla T4 GPUs and 12 GB of RAM resources to accelerate the training process. However, the 12 GB of RAM was not consistently utilized during all model training processes or for every model iteration. A (90%-10%) rate was selected for the train-test split. During the training, we tried several regularization techniques, such as Batch Normalization, L1, and L2 regularization, however the models were overfitted, likely due to the simplicity of our dataset. Given this, we trained the models without regularisation, but we recommend including a regularisation technique for richer datasets.

B. Results

Three look-ahead values (k) were determined for the forecasting:

- $k=1$: model trains to forecast the value of the b_{agg} vector for 96 time slots (equivalent of 1 day) beginning from the next time slot. As the time resolution is 15 min, one step-ahead forecast returns one day forecast of the vector b_{agg} starting from the next 15 min slot. For example, at time step 36 (9 am), the model forecasts b_{agg} from 9am15 until 9 am00 of the next day. This type of forecasts is beneficial for aggregators who want to participate in real or near-real time markets such as FCR, aFRR and mFRR.
- $k=4$: model trains to forecast b_{agg} for one day beginning from the 4th next time slot (i.e., hour-ahead). For instance, at 9 am the model forecasts b_{agg} from 10 am to 9 am45 of the next day. This foresight not only helps aggregators capitalize on intra-day trading opportunities, optimize resource utilization, and avoid potential penalties for imbalances—thereby improving profitability and operational efficiency—but also provides critical insights for bulk system and transmission system operators. Accurate 1-hour ahead forecasts enable these operators to maintain grid stability, efficiently manage load balancing, and anticipate fluctuations in supply and demand.
- $k=48$: model trains to forecast b_{agg} for one day beginning from the 48th next time slot (i.e., half-day-ahead). At 12 pm, the model forecasts b_{agg} for the next day from 00 am00 to 11 pm45. When engaging in day-ahead markets, half-day ahead forecasts are essential for strategic planning and resource allocation. These forecasts provide the necessary information to make informed decisions about energy bids and schedules for the next day.

The parameters of the top two performing Transformer and attention-based CNN-LSTM models are presented in Table II, and the forecasting errors (RMSE) are presented in Table III. The RMSE results are shown alongside a RandomForest (RF) model, which serves as the baseline. Note that the baseline model is not capable of producing multi-variate, multi-step outputs; therefore, three separate models were trained, each corresponding to a different variable.

Model	Parameter	lead=1	lead=4	lead=48
Transformer	N. of layers	4	5	5
	d_model	128	128	128
	N. of heads	8	16	16
	dff	512	128	128
Attention-based CNN-LSTM	N. of CNN layers	1	2	1
	Filters	64	64-128	128
	N. of LSTM layers	2	3	3
	units	64-128	128-128-64	128-128

TABLE II: Parameters of the most performing DL architectures

The results are promising as they demonstrate that using these forecasting algorithms, we were able to reach an acceptable accuracy, less than 6.59% error forecast. Figure 4 shows the results of the prediction for one day selected from the test period data.

TABLE III: Forecasting results.

		RF	CNN-LSTM	Transformer
$k=1$	P_{max}^{agg}	32.31	12.83	10.96
	C_{max}^{agg}	39.84	58.20	35.37
	C_{min}^{agg}	209.10	90.01	60.35
	Average	93.75	53.68	35.56
$k=4$	P_{max}^{agg}	32.7	11.62	9.00
	C_{max}^{agg}	36.06	52.65	30.72
	C_{min}^{agg}	211.04	106.02	48.77
	Average	93.26	56.61	29.5
$k=48$	P_{max}^{agg}	20.6	11.35	9.30
	C_{max}^{agg}	36.06	52.36	33.72
	C_{min}^{agg}	211.04	69.06	50.01
	Average	88.96	44.25	31.01

IV. CASE STUDIES

We demonstrate 2 scenarios on leveraging b_{agg} to gain insights and participate in local energy markets and local flexibility markets. We work with the same dataset as previously and suppose that the aggregator possesses historical data of charging sessions that have relevant information:

- Charging/discharging rates of EV batteries,
- Connection/disconnection times of EV batteries,
- State of charge at arrival and maximum capacity of EV batteries,
- And optionally the desired state of charge at departure.

A. Case study 1: Participation in long-term flexibility contracts

Sustain flexibility service, as defined by Open Networks [26], entails the distribution system operator (DSO) to enter in a long-term contracts with the flexibility service provider (FSP) in which the FSP agrees to alter its power during a pre-defined window. This type of services presents a cost-effective alternative to network reinforcement and is being launched by some DSOs [27, 28] in the UK. Call of tenders are submitted and FSPs send their bids composed of the pair {flexibility, price}.

In our case study, we investigate the potential of the aggregator to engage in a long-term upward flexibility contract with the DSO, and present a method that computes the amount of flexibility the aggregator can bid as a response to a DSO call using the b_{agg} vector.

First, the flexibility is measured as a deviation from a baseline schedule. Here, we assume that the aggregator baseline is an optimal schedule of its resources in response to a day-ahead market price signal:

$$\begin{aligned} \min_{(p_{agg})} \quad & \sum_{t \in \mathcal{T}} \lambda_{imp}^t p_{agg,ch}^t - \lambda_{exp}^t p_{agg,dis}^t \\ \text{s.t.} \quad & A_{agg} p_{agg} - b_{agg} \leq 0 \end{aligned} \quad (4)$$

where $\lambda_{imp}^t / \lambda_{exp}^t$ are the day-ahead import/export prices and $p_{agg} = [p_{agg,ch}^t, p_{agg,dis}^t]^T$ is the charging/discharging aggregated power.

Let us note p_{agg}^{sch} the optimal schedule of the aggregator in response to the market signal, e.g., the result of the optimisation problem (4) and $[T_s, T_e]$ the time window of providing flexibility. The computation of the maximum upward

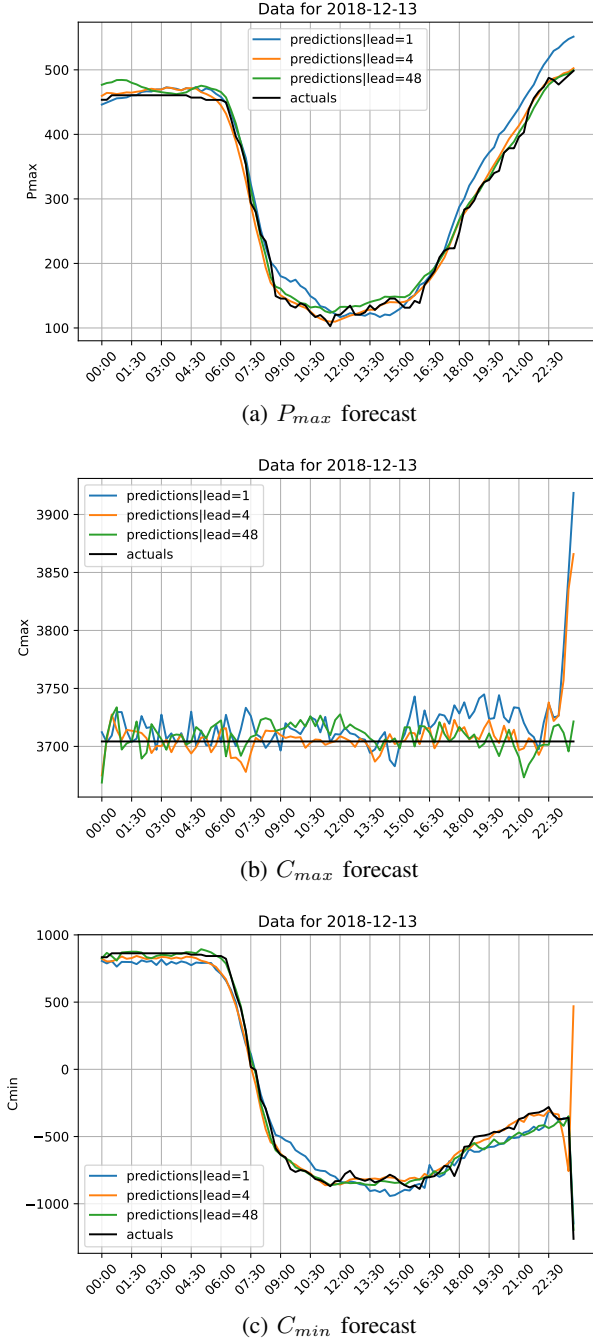


Fig. 4: The forecast of b_{agg} vectors for one day.

flexibility the aggregator can offer in the time window $[T_s, T_e]$ can be retrieved using the following optimisation problem:

$$\begin{aligned}
 & \max_{(flex, p_{agg})} \quad flex \\
 & \text{s.t.} \quad A_{agg} p_{agg} - b_{agg} \leq 0 \\
 & \quad \quad p_{agg}^{sch} - p_{agg} \geq flex, \quad \forall t \in [T_s, T_e]
 \end{aligned} \tag{5}$$

Running this procedure (i.e., problem (4) followed by problem (5)) for available historical data will provide the aggregator with insights into its flexibility capability. Fig. 5a shows the results of running the procedure for days between 01 March 2017 and 28 February 2018. We find that the aggregator can

provide more upward flexibility in the time window 17h30-20h than in 15h-17h, which is expected as this aggregator is managing home-level charging with more availability in the late afternoon than early afternoon. We suppose two scenarios, in one of them the aggregator bids the median value of the flexibility and in the other it bids the third-quantile value. We then assess the reliability of the aggregator to deliver the promised flexibility over the period of 01 March 2018 to 31 December 2018. Table IV shows the results for both scenarios. Successful delivery refers to the cases where the aggregator was able to deliver 90%+ of its bid, partial delivery to [50, 90[% of the bid, and failure of delivery when the delivered flexibility is less than 50% of the agreed capacity. Whether bidding the median or the 3rd quantile value, the aggregator was 99% of the time successful in delivering the bid flexibility. Upon investigating the underlying reasons and closely examining the available flexibility during this second period, as shown in Fig. 5b, we observed a notable increase in the aggregator's flexibility potential. This can be attributed to the inclusion of new EV members joining the project trials, which explains the high success rate of flexibility delivery.

B. Case study 2: Day ahead scheduling of the charging station operation in response to dynamic operating envelop signal

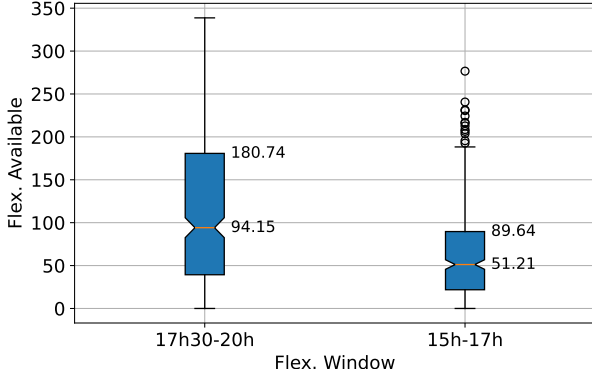
Dynamic operating envelopes (DOEs) define the real-time limits for energy export and import at a connection point [29]. Unlike static limits, DOEs adjust dynamically based on factors such as grid capacity, network conditions, and local demand. This approach enables the seamless integration of renewable energy sources and optimizes grid efficiency.

In this case study, we consider a scenario where the DSO sends day-ahead DOE signals to flexible customers, such as EV aggregators, who adjust their next-day resource scheduling accordingly. The mathematical formulation of this problem involves minimizing the energy bill, subject to the operational constraints of the aggregator and the DOE limits:

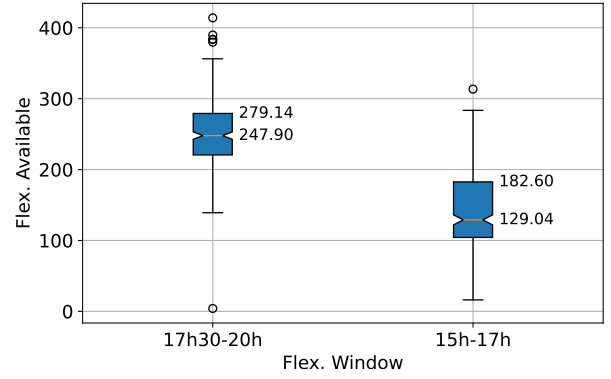
$$\begin{aligned}
 & \min_{p_{agg}} \quad \sum_{t \in \mathcal{T}} \lambda_{imp}^t p_{agg, ch}^t + \lambda_{exp}^t p_{agg, dis}^t \\
 & \text{s.t.} \quad A_{agg} p_{agg} - b_{agg} \leq 0 \\
 & \quad \quad p_{agg, ch}^t \leq p_{doe, imp}^t, \quad \forall t \in \mathcal{T} \\
 & \quad \quad p_{agg, dis}^t \geq p_{doe, exp}^t, \quad \forall t \in \mathcal{T}
 \end{aligned} \tag{6}$$

Where $p_{agg} = [p_{agg, ch}^t, p_{agg, dis}^t]^T$ is the scheduled power output, $p_{doe, imp}^t, p_{doe, exp}^t$ are the import/export DOE limits and $\lambda_{imp}^t, \lambda_{exp}^t$ are the day-ahead import/export prices.

We performed the optimization (6) for both the forecasted b_{agg}^{fore} vector and the actual b_{agg}^{act} vector, resulting in two types of power schedules one using the predicted b_{agg}^{fore} values and one using the b_{agg}^{act} values. The time-varying tariffs *Agile Octopus April 2024 V1* (for imports) and *Agile Outgoing Octopus May 2019* (for exports) were utilized, with the tariffs illustrated in Fig. 6 for November 20, 2024. The selected DOEs for the simulation reflect a system with high solar energy penetration, imposing high (low) import (export) limits around midday, moderate import/export limits in the morning and around late afternoon, and a low (high) import (export)



(a) The period of 01 March 2017 to 28 February 2018.



(b) The period of 01 March 2018 to 31 December 2018.

Fig. 5: Maximum flexibility provision for for two flexibility windows, in the period of feasibility study (left) and period of flexibility activation (right).

TABLE IV: Success rates for flexibility delivery over the period of 01 March 2018 to 31 December 2018.

	Success	17h30-20h Partial success	Failure	Success	15h-17h Partial success	Failure
Median	99.68%	0.0%	0.32%	99.67%	0.0%	0.33%
Q3	99.0%	0.65%	0.32%	92.81%	6.86%	0.32%

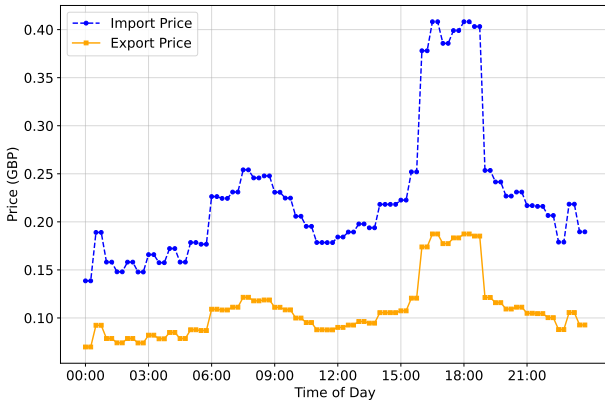


Fig. 6: Import and export energy prices.

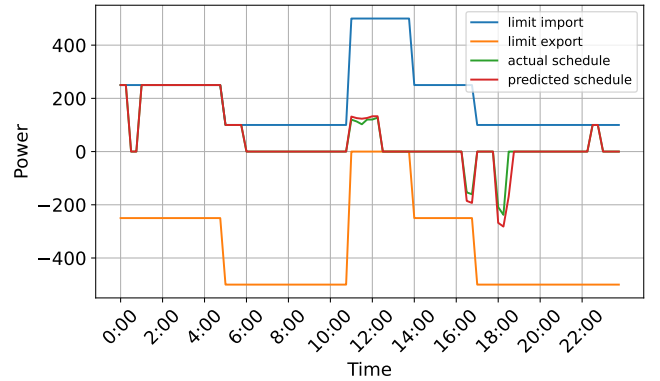


Fig. 7: Aggregator schedule (actual and predicted) in response to DOE signal.

limits in the evenings. The results in Fig. 7 demonstrate the effectiveness of our prediction method for the b vector, showing a slight difference between the two schedules.

V. SUMMARY AND CONCLUSIONS

In this paper, we presented a comprehensive approach for estimating and forecasting V2X flexibility. Our proposed method accurately estimate V2X flexibility potential at an aggregate level and utilize DL architectures to predict future flexibility with high precision. Through two case studies, we demonstrated the practical applicability and effectiveness of our methods in real-world scenarios.

However, while our approach shows promise, several limitations must be addressed to improve the reliability and robustness of V2X flexibility forecasts. A significant challenge is the lack of detailed data, particularly regarding electric vehicle (EV) battery capacity and state of charge at arrival

(SOC_{arr}). Many charging stations currently do not retrieve these critical pieces of information during charging sessions, which are essential for generating reliable V2X flexibility forecasts. To overcome this limitation, there is a pressing need for regulations that mandate the collection of such data and for the development of technical equipment capable of retrieving it.

For future work, it is crucial to collect larger datasets with comprehensive and relevant information. This will not only enable more efficient training of DL methods but also enhance the robustness and accuracy of the forecasts, ultimately contributing to more reliable and actionable insights for energy network operators and other stakeholders in the V2X ecosystem.

APPENDIX A

DL ARCHITECTURES TUNED AND TRAINED

All models were trained using Adam optimiser, with a batch size of 96, dropout rate of 0.1, and up to 500 epochs. The EarlyStopping method was implemented to prevent overfitting, and it allowed the training process to stop automatically if the validation loss does not improve over 50 consecutive epochs. For CNN layers in Attention-based CNN-LSTM models, the kernel size was set to 3, pool size to 2, padding to ‘same’ and activation function to Relu. The activation function of LSTM layers of the same model was set to Relu as well.

Model	Layers
simpleRNN	Conv1D(filters=32, kernel size=24*4)
	SimpleRNN(filters=64)
	SimpleRNN(filters=128)
	Flatten
	RepeatVector(96)
LSTM	TimeDistributed(Dense: filters=3)
	Conv1D(filters=32, kernel size=24*4)
	Conv1D(filters=63, kernel size=1)
	LSTM(filters=32)
	Flatten
	RepeatVector(96)
	LSTM(filters=64)
bi-LSTM	LSTM(filters=32)
	TimeDistributed(Dense: filter=3)
	Conv1D(filters=32, kernel size=24*4)
	Conv1D(filters=64, kernel size=1)
	Bidirectional(LSTM: filters=128)
	Bidirectional(LSTM: filters=64)
	RepeatVector(96)
	LSTM(filters=128)
GRU	LSTM(filters=64)
	LSTM(filters=32)
	TimeDistributed(Dense: filter=3)
	Conv1D(filters=32, kernel size=24*4)
	GRU(filters=64)
Attention-based CNN-LSTM	GRU(filters=128)
	flatten
	RepeatVector(96)
	TimeDistributed(Dense: filters=3)
	LSTM(filters=50)
	Attention layer
	RepeatVector(35)
Transformer	Concatenate(LSTM, Attention)
	LSTM(filters=128)
	Dense(filters=96*3)
	Reshape(filters=96*3)
Transformer	Transformer(layers=4, d_model=128, heads=8, dff=512)

TABLE V: DL architectures considered for the first round evaluation.

Model	Parameter	Range/Set
Transformer	N. of layers	{4, 5, 6}
	d_model	{32, 64, 128}
	N. of heads	{4, 8, 16}
	dff	{128, 256, 512}
Attention-based CNN-LSTM	N. of CNN layers	{1, 2}
	Filters	{32, 64, 128}
	N. of LSTM layers	{2, 3}
	units	{64, 128}

TABLE VI: DL architectures and parameters tuned for the second round evaluation.

ACKNOWLEDGEMENTS

The authors would like to thank the funding for DriVe2X research and innovation project from the European Commission and the UKRI, with grant numbers 101056934 and 10055673, respectively.

REFERENCES

- [1] R. Zhang and S. Fujimori, “The role of transport electrification in global climate change mitigation scenarios,” *Environmental Research Letters*, vol. 15, no. 3, p. 034019, 2020.
- [2] P. G. Pereirinha, M. González, I. Carrilero, D. Anseán, J. Alonso, and J. C. Viera, “Main trends and challenges in road transportation electrification,” *Transportation Research Procedia*, vol. 33, pp. 235–242, 2018, xIII Conference on Transport Engineering, CIT2018.
- [3] R. Álvarez Fernández, “Method for assessing the environmental benefit of road transport electrification and its influence on greenhouse gas inventories,” *Journal of Cleaner Production*, vol. 218, pp. 476–485, 2019.
- [4] E. S. Trust, “Forecasting public electric vehicle charging demand: A guide for local authorities in england prepared by the local government support programme,” Energy Saving Trust, Tech. Rep., 2022.
- [5] K. J. Dyke, N. Schofield, and M. Barnes, “The impact of transport electrification on electrical networks,” *IEEE Transactions on Industrial Electronics*, vol. 57, no. 12, pp. 3917–3926, 2010.
- [6] A. Tavakoli, S. Saha, M. T. Arif, M. E. Haque, N. Mendis, and A. M. Oo, “Impacts of grid integration of solar pv and electric vehicle on grid stability, power quality and energy economics: a review,” *IET Energy Systems Integration*, vol. 2, no. 3, pp. 243–260, 2020.
- [7] A. M. Haidar, K. M. Muttaqi, and D. Sutanto, “Technical challenges for electric power industries due to grid-integrated electric vehicles in low voltage distributions: A review,” *Energy Conversion and Management*, vol. 86, pp. 689–700, 2014.
- [8] H. Lund and W. Kempton, “Integration of renewable energy into the transport and electricity sectors through v2g,” *Energy Policy*, vol. 36, no. 9, pp. 3578–3587, 2008.
- [9] W. Liu, W. Hu, H. Lund, and Z. Chen, “Electric vehicles and large-scale integration of wind power – the case of inner mongolia in china,” *Applied Energy*, vol. 104, pp. 445–456, 2013.
- [10] M. Yuan, J. Z. Thellufsen, H. Lund, and Y. Liang, “The electrification of transportation in energy transition,” *Energy*, vol. 236, p. 121564, 2021.
- [11] M.-J. Jang, T. Kim, and E. Oh, “Data-driven modeling of vehicle-to-grid flexibility in korea,” *Sustainability*, vol. 15, no. 10, 2023.
- [12] C. Devellder, N. Sadeghianpourhamami, M. Strobbe, and N. Refa, “Quantifying flexibility in ev charging as dr potential: Analysis of two real-world data sets,” in *2016 IEEE International Conference on Smart Grid Communications (SmartGridComm)*, 2016, pp. 600–605.
- [13] A. Bartolini and G. Hug, “An open-data based framework to estimate ev demand and attainable flexibility and application to the case of singapore,” *Sustainable Energy, Grids and Networks*, vol. 36, p. 101196, 2023.
- [14] H. Zhang, Z. Hu, Z. Xu, and Y. Song, “Evaluation of achievable vehicle-to-grid capacity using aggregate pev model,” *IEEE Transactions on Power Systems*, vol. 32, no. 1, pp. 784–794, 2017.
- [15] L. Wang, J. Kwon, N. Schulz, and Z. Zhou, “Evaluation of aggregated ev flexibility with tso-dso coordination,” *IEEE Transactions on Sustainable Energy*, vol. 13, no. 4, pp. 2304–2315, 2022.
- [16] T. Harighi, A. Borghetti, F. Napolitano, and F. Tossani, “Flexibility modeling for parking lots with multiple ev charging stations,” *Electric Power Systems Research*, vol. 234, p. 110732, 2024.
- [17] M. Zhang, Y. Xu, X. Shi, and Q. Guo, “A fast polytope-based approach for aggregating large-scale electric vehicles in the joint market under uncertainty,” *IEEE Transactions on Smart Grid*, vol. 15, no. 1, pp. 701–713, 2024.
- [18] M. Voß, M. Wilhelm, and S. Albayrak, “Application independent flexibility assessment and forecasting for controlled ev charging,” in *SMARTGREENS*, 2018, pp. 108–119.
- [19] J. Huber, D. Dann, and C. Weinhardt, “Probabilistic forecasts of time and energy flexibility in battery electric vehicle charging,” *Applied Energy*, vol. 262, p. 114525, 2020.
- [20] E. Genov, C. D. Cauwer, G. V. Kriekinge, T. Coosemans, and M. Mesagie, “Forecasting flexibility of charging of electric vehicles: Tree and cluster-based methods,” *Applied Energy*, vol. 353, p. 121969, 2024.
- [21] N. K. Panda and S. H. Tindemans, “Quantifying the aggregate flexibility of ev charging stations for dependable congestion management

- products: A dutch case study,” 2024. [Online]. Available: <https://arxiv.org/abs/2403.13367>
- [22] J. Hu, H. Zhou, Y. Zhou, H. Zhang, L. Nordström, and G. Yang, “Flexibility prediction of aggregated electric vehicles and domestic hot water systems in smart grids,” *Engineering*, vol. 7, no. 8, pp. 1101–1114, 2021.
- [23] S. Barot and J. A. Taylor, “A concise, approximate representation of a collection of loads described by polytopes,” *International Journal of Electrical Power & Energy Systems*, vol. 84, pp. 55–63, 2017.
- [24] N. G. ESO, “Electric nation data,” <https://www.nationalgrid.co.uk/downloads-view/81646>, 2019, accessed: 2024-10-03.
- [25] C. Essayeh and T. Morstyn, “Oplem: Open platform for local energy markets,” *Applied Energy*, vol. 373, p. 123848, 2024.
- [26] E. N. Association, “Active power services implementation plan,” <https://www.energynetworks.org/assets/images/Resource%20library/ON-WS1A-P3%20Active%20Power%20Services%20-%20Final%20Implementation%20Plan-PUBLISHED.23.12.20.pdf>, 2020.
- [27] Scottish and southern Electricity Networks, “Flexibility webinar global call,” <https://www.ssen.co.uk/globalassets/our-services/flexibility-services-document-library/current-tenders/global-call-webinar-slides-september-2023.pdf>, 2023.
- [28] U. P. Networks, “Flexibility product update,” https://d11f1oz5vvd9r.cloudfront.net/app/uploads/2024/03/Products-Update_240228.pdf, 2024.
- [29] C. Essayeh and T. Morstyn, “Dynamic operating envelopes in distribution networks: A reliable computation,” in *2024 IEEE Power & Energy Society General Meeting (PESGM)*, 2024, pp. 1–5.